Acta Mech 229, 4895–4913 (2018)
https://doi.org/10.1007/s00707-018-2289-x

ORIGINAL PAPER

R. Bagheri · M. M. Monfared

Magneto-electro-elastic analysis of a strip containing multiple embedded and edge cracks under transient loading

Received: 17 November 2017 / Revised: 11 August 2018 / Published online: 22 October 2018

Abstract This paper deals with the dynamic behavior of a magneto-electro-elastic strip weakened by multiple horizontal, vertical, and edge cracks within the framework of linear magneto-electro-elasticity. The analysis is based on stress and the magneto-electrical fields caused by horizontal and vertical Volterra-type screw dislocation in a medium. The problem was formulated through Fourier and Laplace transforms into singular integral equations in which the unknown variables are the jumps of displacement and magneto-electrical potential across the crack surface. The dislocation densities and the numerical Laplace inversion are then employed in order to derive the dynamic field intensity factors at the crack tips for both permeable and impermeable cracks. The effects of length and position of the cracks on the dynamic field intensity factors and interaction between the two cracks are investigated. Furthermore, the results show that, for a fixed value of mechanical load, the dynamic field intensity factor at the crack tips depends on the magnitude and direction of the applied magneto-electrical load.

1 Introduction

Magneto-electro-elastic materials and structures that combine piezoelectric and piezomagnetic phases have received significant attention due to the potential for designing adaptive structures that are both light in weight and possess adaptive control capabilities. Because of their brittleness, cracks in these materials are greatly concerned. Thus, the fracture analysis of this class of materials containing defects such as cracks is an important problem. Cracked magneto-electro-elastic material clearly consists of multiple cracks with an extremely high crack density. Therefore, the interaction between several cracks in magneto-electro-elastic materials under the permeable and impermeable conditions on the crack surfaces plays an important role in the analysis and design of smart structures. It is worth noting that different magneto-electrical boundary conditions on the crack surfaces lead to diverse results for the fracture behavior of these materials. However, most of the fracture analyses for smart materials are related to the static or quasi-static loading. But, it may be very important to study the transient loading condition in these materials.

The static or quasi-static fracture analysis in a smart material has drawn significant attention in recent years [1–6]. A finite crack in an infinite piezoelectric medium under transient electro-mechanical loads has been studied by Chen and Karihaloo [7]. In this paper, the effects of directions of electrical loads upon dynamic stress intensity factors (DSIFs) have been studied. The paper by Li [8] was concerned with a semi-infinite cracked piezoelectric material due to a point load magneto-electrical impact at the crack surfaces. The mechanical

R. Bagheri (✉)
Department of Mechanical Engineering, Mechatronics Faculty, Karaj Branch, Islamic Azad University, Karaj, Alborz, Iran
E-mail: r.bagheri@kiau.ac.ir

M. M. Monfared
Department of Mechanical Engineering, Hashtgerd Branch, Islamic Azad University, Karaj, Alborz, Iran

strain energy release rate was computed, and the dynamic intensity factors of the electro-elastic field were investigated. The article by Gu et al. [9] dealt with the problem of an interface crack between dissimilar piezoelectric layers under magneto-electrical impacts. The effects of the loading ratio, the geometry of crack arrangement and the material properties on the field intensity factors were studied. The out-of-plane transient deformation of an infinite FGM with a finite crack was examined by Zhang et al. [10]. The influences of the material gradients of the FGM on the DSIFs and their dynamic overshoot corresponding with the static SIFs were discussed. The dynamic anti-plane mechanical and in-plane electric and magnetic crack problem of a magneto-electro-elastic medium was the subject of the study by Li [11]. They investigated the effects of the material properties and applied electro-magnetic impacts on the dynamic intensity factors. Feng and Su [12] analyzed the transient response of a functionally graded magneto-electro-elastic strip containing an internal crack perpendicular to the boundary. By using integral transforms and dislocation density functions, the problem reduced to Cauchy-kind singular integral equations. Su et al. [13] investigated the problem of interface cracks between dissimilar magneto-electro-elastic strips under anti-plane mechanical and in-plane magneto-electrical impacts. In this study, a magneto-electrical permeable boundary condition was adopted. The transient problem was analyzed by Yong and Zhou [14] for a magneto-electro-elastic strip containing an impermeable crack perpendicular to the boundary. The influences of the geometric parameters and the magneto-electrical impacts on the dynamic response were investigated. Garcı'a-Sa'nchez et al. [15] performed theoretical studies to evaluate the DSIF of cracked two-dimensional (2-D), homogeneous, and linear piezoelectric solids. They investigated the effects of the mechanical and the electrical impact loading on the fracture behavior of the medium. Chen [16] studied the dynamic response of a permeable and impermeable crack propagating in a magneto-electro-elastic solid subjected to the mixed loads.

The above-mentioned problems are restricted to one or two periodic cracks. The transient analysis of several defects such as embedded and edge cracks has never been performed for a magneto-electro-elastic strip, but recently by use of the distribution dislocation technique (DDT) articles, which possess several cracks examined in them, are published. DDT is a powerful semi-analytical technique for calculating accurate solutions to anti-plane and in-plane crack problems based on the principle of superposition. A brief review of relevant articles is given below.

Several cracks in an orthotropic substrate reinforced by functionally graded materials coating with DDT in order to obtain DSIF under time-harmonic excitation were examined by Monfared and Ayatollahi [17]. The influence of the angular frequency, crack lengths, and material properties were studied on the DSIF. Interaction between multiple moving cracks with arbitrary arrangement in a functionally graded magneto-electro-elastic strip under anti-plane mechanical and in-plane magneto-electrical loading was studied by Bagheri et al. [18]. The DSIF associated with crack tips was calculated by a numerical inverse Laplace scheme. Vafa et al. [19] used the DDT and the numerical inversion method to obtain the transient response of the FG strip weakened by several horizontal cracks.

The problem of a circular orthotropic bar with several cracks under torsional transient loading was investigated by Hassani and Monfared [20]. They use the Saint-Venant torsion theory and the DDT for an analysis of multiple cracks. Recently Bagheri [21] obtained field intensity factors for multiple cracks in a piezoelectric half plane under transient loading. This author employed the DDT to solve the problem.

According to the above literature review, there is not a promising examination regarding the transient analysis of several kinds of cracks such as multiple embedded and edge cracks in the magneto-electro-elastic strip. In this study, we consider the dynamic behavior of a magneto-electro-elastic strip weakened by multiple cracks under time-dependent loads. Both the permeable and impermeable boundary conditions are adopted. The integral transforms and DDT in conjunction with the numerical Stehfest inversion method are used in order to obtain the Cauchy singular integral equations which are solved numerically, so the dynamic field intensity factors are determined.

2 Statement of the problem

2.1 Horizontal dislocation cuts

We consider a magneto-electro-elastic strip with magneto-electro-mechanical dislocation which lies at a point having coordinates (ζ, η) (see Fig. 1). In this Section, a basic formulation of the problem with horizontal dislocation cut is derived, and the associated fundamental solutions will be used to solve several horizontal cracks in the numerical Section.

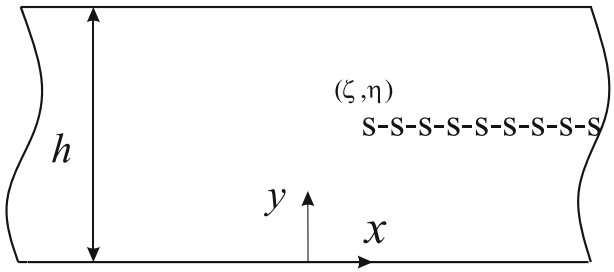

Fig. 1 Schematic view of the magneto-electro-elastic strip with horizontal dislocation cut

The anti-plane displacements and the in-plane magneto-electrical fields are considered, which are independent of z, i.e.,

$$u = 0, v = 0, w = w(x, y, t), \tag{1.1}$$
$$E_x = E_x(x, y, t), E_y = E_y(x, y, t), E_z = 0, \tag{1.2}$$
$$H_X = H_X(x, y, t), H_Y = H_Y(x, yt), H_Z = 0, \tag{1.3}$$

in which the electric and magnetic fields vector can be written in terms of the electric and magnetic potentials, $\phi(x, y)$ and $\psi(x, y)$, by the following forms:

$$E_x = -\partial\phi(x, y)/\partial x, \qquad E_y = -\partial\phi(x, y)/\partial y, \tag{2.1}$$
$$H_x = -\partial\psi(x, y)/\partial x, \qquad H_y = -\partial\psi(x, y)/\partial y. \tag{2.2}$$

In this case, the non-vanishing constitutive relations based on the linearly magneto-electro-elastic theory undergoing out-of-plane displacement and the in-plane magneto-electrical fields become:

$$\tau_{zx} = c_{44}\partial w/\partial x + e_{15}\partial\phi/\partial x + h_{15}\partial\psi/\partial x, \tag{3.1}$$
$$\tau_{zy} = c_{44}\partial w/\partial y + e_{15}\partial\phi/\partial y + h_{15}\partial\psi/\partial y, \tag{3.2}$$
$$D_x = e_{15}\partial w/\partial x - d_{11}\partial\phi/\partial x - \beta_{11}\partial\psi/\partial x, \tag{3.3}$$
$$D_y = e_{15}\partial w/\partial y - d_{11}\partial\phi/\partial y - \beta_{11}\partial\psi/\partial y, \tag{3.4}$$
$$B_x = h_{15}\partial w/\partial x - \beta_{11}\partial\phi/\partial x - \gamma_{11}\partial\psi/\partial x, \tag{3.5}$$
$$B_y = h_{15}\partial w/\partial y - \beta_{11}\partial\phi/\partial y - \gamma_{11}\partial\psi/\partial y \tag{3.6}$$

where c_{44}, e_{15}, h_{15}, and β_{11} are the elastic shear modulus, piezoelectric, piezomagnetic and electro-magnetic constants, respectively; d_{11} and γ_{11} are dielectric permittivities and magnetic permeabilities, respectively. D_x, D_y are the electric displacement components and B_x,B_y the magnetic displacement components, respectively. By neglecting body forces and magneto-electrical charge density, the dynamic out-of-plane governing equations for the magneto-electro-elastic materials are given as follows:

$$\partial\tau_{zx}/\partial x + \partial\tau_{zy}/\partial y = \rho\partial^2 w(x, y, t)/\partial t^2, \tag{4.1}$$
$$\partial D_x/\partial x + \partial D_y/\partial y = 0, \tag{4.2}$$
$$\partial B_x/\partial x + \partial B_y/\partial y = 0 \tag{4.3}$$

where ρ is the density of the magneto-electro-elastic material. Substituting Eqs. (3.1–3) into the equations of motion and Eqs. (3.3,4) and (3.5,6) into the equilibrium equations of electric displacements and magnetic inductions, respectively, yields

$$c_{44}\nabla^2 w + e_{15}\nabla^2\phi + h_{15}\nabla^2\psi = \rho\frac{\partial^2}{\partial t^2}w(x, y, t), \tag{5.1}$$
$$e_{15}\nabla^2 w - d_{11}\nabla^2\phi - \beta_{11}\nabla^2\psi = 0, \tag{5.2}$$
$$h_{15}\nabla^2 w - \beta_{11}\nabla^2\phi - \gamma_{11}\nabla^2\psi = 0 \tag{5.3}$$

where $\nabla^2 = \partial^2/\partial x^2 + \partial^2/\partial y^2$ is the plane Laplacian operator. We can introduce the scalar potential Bleustein function [22] as follows:

$$\begin{aligned} \bar{\phi} &= \phi - \alpha_2 w, \\ \bar{\psi} &= \psi - \alpha_3 w \end{aligned} \tag{6}$$

in which $\alpha_2 = (\gamma_{11}e_{15} - \beta_{11}h_{15})/(d_{11}\gamma_{11} - \beta_{11}^2)$ and $\alpha_3 = (d_{11}h_{15} - \beta_{11}e_{15})/(d_{11}\gamma_{11} - \beta_{11}^2)$, and one may transform Eqs. (5.1–3) into the following simple forms:

$$\begin{aligned} \nabla^2 w &= S_T^2 \partial^2 w/\partial t^2, \\ \nabla^2 \bar{\phi} &= 0. \\ \nabla^2 \bar{\psi} &= 0 \end{aligned} \tag{7}$$

where S_T is defined by $S_T = 1/C_T$, and $C_T = \sqrt{\tilde{c}_{44}/\rho}$ is the out-of-plane shear wave velocity and $\tilde{c}_{44} = c_{440} + e_{150}\alpha_2 + h_{150}\alpha_3$ is the magneto-electro-elastic constant. From the constitutive equations (3.1–6) and (6), we can get

$$\tau_{xz} = \tilde{c}_{44}\partial w/\partial x + e_{15}\partial\bar{\phi}/\partial x + h_{15}\partial\bar{\psi}/\partial x, \tag{8.1}$$
$$\tau_{yz} = \tilde{c}_{44}\partial w/\partial y + e_{15}\partial\bar{\phi}/\partial y + h_{15}\partial\bar{\psi}/\partial y, \tag{8.2}$$
$$D_x = -d_{11}\partial\bar{\phi}/\partial x - \beta_{11}\partial\bar{\psi}/\partial x, \tag{8.3}$$
$$D_y = -d_{11}\partial\bar{\phi}/\partial y - \beta_{11}\partial\bar{\psi}/\partial y, \tag{8.4}$$
$$B_x = -\beta_{11}\partial\bar{\phi}/\partial x - \gamma_{11}\partial\bar{\psi}/\partial x, \tag{8.5}$$
$$B_y = -\beta_{11}\partial\bar{\phi}/\partial y - \gamma_{11}\partial\bar{\psi}/\partial y \tag{8.6}$$

Let magneto-electro-mechanical dislocations with time-dependent Burgers vectors $b_z(t)$, $b_\phi(t)$ and $b_\psi(t)$ be situated at a point with coordinates (ζ, η) as depicted in Fig. 1. The horizontal dislocation cut is $x > \zeta$, $y = \eta$.

In fracture analysis of magneto-electro-elastic materials, two models of the electro-magnetic boundary conditions along the crack faces are of significance. Generally, there are two well-accepted electro-magnetic boundary conditions, namely the permeable and impermeable boundary conditions. The permeable boundary condition represents the case where the crack faces are in complete contact. It is worth noting that the impermeable conditions are adopted by introducing the jumps of electric and magnetic potential across the dislocation cut. Thus, the mechanical and magneto-electrical dislocation conditions can be described as:

$$\begin{aligned} w(x,\eta^+,t) - w(x,\eta^-,t) &= b_z(t)H(x-\zeta), \\ \bar{\phi}(x,\eta^+,t) - \bar{\phi}(x,\eta^-,t) &= [b_\phi(t) - \alpha_2 b_z(t)]H(x-\zeta), \\ \bar{\psi}(x,\eta^+,t) - \bar{\psi}(x,\eta^-,t) &= [b_\psi(t) - \alpha_3 b_z(t)]H(x-\zeta), \\ \tau_{zy}(x,\eta^+,t) &= \tau_{zy}(x,\eta^-,t), \\ D_y(x,\eta^+,t) &= D_y(x,\eta^-,t), \\ B_y(x,\eta^+,t) &= B_y(x,\eta^-,t) \end{aligned} \tag{9}$$

where $H(.)$ is the Heaviside step function. Although the jumps in the electric and magnetic potentials are not a type of dislocation, they are referred here as electric and magnetic dislocations for convenience. In addition, the traction and magneto-electrical displacements free boundary condition on the strip boundary can be written as:

$$\begin{aligned} \tau_{zy}(x,h,t) &= 0, \\ D_y(x,h,t) &= 0, \\ B_y(x,h,t) &= 0, \\ \tau_{zy}(x,0,t) &= 0, \\ D_y(x,0,t) &= 0, \\ B_y(x,0,t) &= 0. \end{aligned} \tag{10}$$

By applying Laplace transform together with Fourier transform to Eq. (7) and assuming that the magneto-electro-elastic strip is stationary at time $t = 0$, the solution of the governing Eq. (7) is given by:

$$\begin{aligned}
W^*(\omega, y, s) &= A_1(\omega, s)e^{-y\beta} + A_2(\omega, s)e^{+y\beta} \quad 0 \le y \le \eta,\\
W^*(\omega, y, s) &= A_3(\omega, s)e^{-y\beta} + A_4(\omega, s)e^{+y\beta} \quad \eta \le y \le h,\\
\Phi^*(\omega, y, s) &= B_1(\omega, s)e^{-y|\omega|} + B_2(\omega, s)e^{+y|\omega|} \quad 0 \le y \le \eta,\\
\Phi^*(\omega, y, s) &= B_3(\omega, s)e^{-y|\omega|} + B_4(\omega, s)e^{+y|\omega|} \quad \eta \le y \le h,\\
\psi^*(\omega, y, s) &= C_1(\omega, s)e^{-y|\omega|} + C_2(\omega, s)e^{+y|\omega|} \quad 0 \le y \le \eta,\\
\Phi^*(\omega, y, s) &= C_3(\omega, s)e^{-y|\omega|} + C_4(\omega, s)e^{+y|\omega|} \quad \eta \le y \le h
\end{aligned} \tag{11}$$

where

$$\beta = \sqrt{\omega^2 + (S_T s)^2}. \tag{12}$$

By applying conditions (9)–(10) the unknown functions $A_i, B_i, C_i, i = 1, 2, 3, 4$ are determined which are explained in detail in the "Appendix." The results are then substituted into the constitutive equations (8.1–6), and by virtue of the inverse complex Fourier transform the expressions for the components of the stress, electric, and magnetic displacements are obtained. Then splitting the integrals into odd and even parts with respect to the parameter ω, the Laplace transform of the stress and magneto-electrical displacement is simplified. A simple analysis leads to the expressions for the stress and magneto-electrical displacement in the Laplace transform domain which is not detailed here. The final results are as follows:

$$\begin{aligned}
\bar{\tau}_{zy}(x, y, s) &= \frac{b_z(s)\tilde{c}_{44}}{\pi}\int_0^\infty \frac{\beta\sinh(\beta(\eta-h))\sinh(\beta y)}{\omega\sinh(\beta h)}\sin(\omega(x-\zeta))d\omega\\
&\quad + \frac{b_\phi(s)e_{15} + b_\psi(s)h_{15} - (e_{15}\alpha_2 + h_{15}\alpha_3)b_z(s)}{\pi}\\
&\quad \int_0^\infty \frac{\sinh(\omega(\eta-h))\sinh(\omega y)}{\sinh(\omega h)}\sin(\omega(x-\zeta))d\omega, \quad 0 \le y \le \eta,\\
\bar{\tau}_{zy}(x, y, s) &= \frac{b_z(s)\tilde{c}_{44}}{\pi}\int_0^\infty \frac{\beta\sinh(\beta\eta)\sinh(\beta(y-h))}{\omega\sinh(\beta h)}\sin(\omega(x-\zeta))d\omega\\
&\quad + \frac{b_\phi(s)e_{15} + b_\psi(s)h_{15} - (e_{15}\alpha_2 + h_{15}\alpha_3)b_z(s)}{\pi}\\
&\quad \int_0^\infty \frac{\sinh(\omega\eta)\sinh(\omega(y-h))}{\sinh(\omega h)}\sin(\omega(x-\zeta))d\omega, \quad \eta \le y \le h,\\
\bar{D}_y(x, y, s) &= \frac{b_z(s)(d_{11}\alpha_2 + \beta_{11}\alpha_3) - b_\phi(s)d_{11} - b_\psi(s)\beta_{11}}{\pi}\\
&\quad \int_0^\infty \frac{\sinh(\omega(\eta-h))\sinh(\omega y)}{\sinh(\omega h)}\sin(\omega(x-\zeta))d\omega, \quad 0 \le y \le \eta,\\
\bar{D}_y(x, y, s) &= \frac{b_z(s)(d_{11}\alpha_2 + \beta_{11}\alpha_3) - b_\phi(s)d_{11} - b_\psi(s)\beta_{11}}{\pi}\\
&\quad \int_0^\infty \frac{\sinh(\omega\eta)\sinh(\omega(y-h))}{\sinh(\omega h)}\sin(\omega(x-\zeta))d\omega, \quad \eta \le y \le h,\\
\bar{B}_y(x, y, s) &= \frac{b_z(s)(\beta_{11}\alpha_2 + \gamma_{11}\alpha_3) - b_\phi(s)\beta_{11} - b_\psi(s)\gamma_{11}}{\pi}\\
&\quad \int_0^\infty \frac{\sinh(\omega(\eta-h))\sinh(\omega y)}{\sinh(\omega h)}\sin(\omega(x-\zeta))d\omega, \quad 0 \le y \le \eta,\\
\bar{B}_y(x, y, s) &= \frac{b_z(s)(\beta_{11}\alpha_2 + \gamma_{11}\alpha_3) - b_\phi(s)\beta_{11} - b_\psi(s)\gamma_{11}}{\pi}\\
&\quad \int_0^\infty \frac{\sinh(\omega\eta)\sinh(\omega(y-h))}{\sinh(\omega h)}\sin(\omega(x-\zeta))d\omega, \quad \eta \le y \le h.
\end{aligned} \tag{13}$$

The above stress and magneto-electrical displacement components are singular at the dislocation location. For this, it is sufficient to investigate the asymptotic behavior of the integrands of the integrals in (13). Because the integrands are continuous functions of ω and also are bounded at $\omega = 0$, the singularity must occur as ω tends to infinity. By adding and subtracting the asymptotic expressions of the integrands using asymptotic expressions for large values of ω, we find:

$$\begin{aligned}
\bar{\tau}_{zy}(x, y, s) = {} & \frac{b_z(s)\tilde{c}_{44}}{\pi} \\
& \left\{ \int_0^\infty \left[\frac{\beta \sinh(\beta(\eta - h)) \sinh(\beta y)}{\omega \sinh(\beta h)} + \frac{e^{-\omega(\eta - y)}}{2} \right] \right. \\
& \left. \sin(\omega(x - \zeta)) d\omega - \frac{(x - \zeta)}{2[(x - \zeta)^2 + (y - \eta)^2]} \right\} \\
& + \frac{b_\phi(s) e_{15} + b_\psi(s) h_{15} - (e_{15}\alpha_2 + h_{15}\alpha_3) b_z(s)}{\pi} \\
& \times \left\{ \int_0^\infty \left[\frac{\sinh(\omega(\eta - h)) \sinh(\omega y)}{\sinh(\omega h)} + \frac{e^{-\omega(\eta - y)}}{2} \right] \right. \\
& \left. \sin(\omega(x - \zeta)) d\omega - \frac{(x - \zeta)}{2[(x - \zeta)^2 + (y - \eta)^2]} \right\}, \quad 0 \le y \le \eta, \\
\bar{\tau}_{zy}(x, y, s) = {} & \frac{b_z(s)\tilde{c}_{44}}{\pi} \left\{ \int_0^\infty \left[\frac{\beta \sinh(\beta \eta) \sinh(\beta(y - h))}{\omega \sinh(\beta h)} + \frac{e^{\omega(\eta - y)}}{2} \right] \right. \\
& \left. \sin(\omega(x - \zeta)) d\omega - \frac{(x - \zeta)}{2[(x - \zeta)^2 + (y - \eta)^2]} \right\} \\
& + \frac{b_\phi(s) e_{15} + b_\psi(s) h_{15} - (e_{15}\alpha_2 + h_{15}\alpha_3) b_z(s)}{\pi} \\
& \times \left\{ \int_0^\infty \left[\frac{\sinh(\omega \eta) \sinh(\omega(y - h))}{\sinh(\omega h)} + \frac{e^{\omega(\eta - y)}}{2} \right] \right. \\
& \left. \sin(\omega(x - \zeta)) d\omega - \frac{(x - \zeta)}{2[(x - \zeta)^2 + (y - \eta)^2]} \right\}, \quad \eta \le y \le h,
\end{aligned}$$

$$\begin{aligned}
\bar{D}_y(x, y, s) = {} & \frac{b_z(s)(d_{11}\alpha_2 + \beta_{11}\alpha_3) - b_\phi(s) d_{11} - b_\psi(s)\beta_{11}}{\pi} \\
& \times \left\{ \int_0^\infty \left[\frac{\sinh(\omega(\eta - h)) \sinh(\omega y)}{\sinh(\omega h)} + \frac{e^{-\omega(\eta - y)}}{2} \right] \right. \\
& \left. \sin(\omega(x - \zeta)) d\omega - \frac{(x - \zeta)}{2[(x - \zeta)^2 + (y - \eta)^2]} \right\}, \quad 0 \le y \le \eta, \\
\bar{D}_y(x, y, s) = {} & \frac{b_z(s)(d_{11}\alpha_2 + \beta_{11}\alpha_3) - b_\phi(s) d_{11} - b_\psi(s)\beta_{11}}{\pi} \\
& \times \left\{ \int_0^\infty \left[\frac{\sinh(\omega \eta) \sinh(\omega(y - h))}{\sinh(\omega h)} + \frac{e^{\omega(\eta - y)}}{2} \right] \right. \\
& \left. \sin(\omega(x - \zeta)) d\omega - \frac{(x - \zeta)}{2[(x - \zeta)^2 + (y - \eta)^2]} \right\}, \quad \eta \le y \le h, \\
\bar{B}_y(x, y, s) = {} & \frac{b_z(s)(\beta_{11}\alpha_2 + \gamma_{11}\alpha_3) - b_\phi(s)\beta_{11} - b_\psi(s)\gamma_{11}}{\pi} \\
& \times \left\{ \int_0^\infty \left[\frac{\sinh(\omega(\eta - h)) \sinh(\omega y)}{\sinh(\omega h)} + \frac{e^{-\omega(\eta - y)}}{2} \right] \right.
\end{aligned}$$

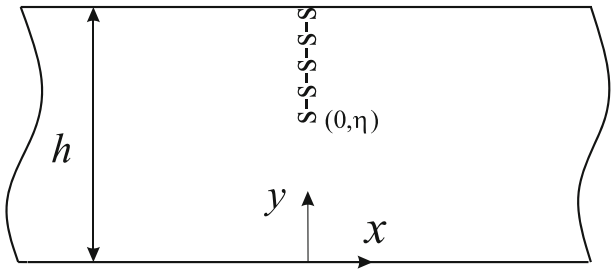

Fig. 2 Schematic view of the medium with vertical dislocation cut

$$\left.\sin(\omega(x-\zeta))d\omega - \frac{(x-\zeta)}{2[(x-\zeta)^2+(y-\eta)^2]}\right\}, \quad 0 \le y \le \eta,$$

$$\bar{B}_y(x,y,s) = \frac{b_z(s)(\beta_{11}\alpha_2+\gamma_{11}\alpha_3) - b_\phi(s)\beta_{11} - b_\psi(s)\gamma_{11}}{\pi} \times \left\{\int_0^\infty \left[\frac{\sinh(\omega\eta)\sinh(\omega(y-h))}{\sinh(\omega h)} + \frac{e^{\omega(\eta-y)}}{2}\right]\right.$$

$$\left.\sin(\omega(x-\zeta))d\omega - \frac{(x-\zeta)}{2[(x-\zeta)^2+(y-\eta)^2]}\right\}, \quad \eta \le y \le h. \tag{14}$$

2.2 Vertical dislocation cuts

In this part of the study, at first, the stress fields and magneto-electrical displacement components in a magneto-electro-elastic strip with vertical dislocation cut are derived. Then, these solutions will be used to determine the dynamic field intensity factors for the multiple vertical and edge cracks in the numerical section. A magneto-electro-elastic strip with thickness h under consideration is described in Fig. 2. The vertical dislocation cut is $x = 0$, $y > \eta$.

The conditions representing the vertical screw dislocations cut and boundary conditions are expressed as follows:

$$\begin{aligned}
w(0^+,y,t) - w(0^-,y,t) &= b_z(t)H(y-\eta),\\
\bar{\phi}(0^+,y,t) - \bar{\phi}(0^-,y,t) &= [b_\phi(t) - \alpha_2 b_z(t)]H(y-\eta),\\
\bar{\psi}(0^+,y,t) - \bar{\psi}(0^-,y,t) &= [b_\psi(t) - \alpha_3 b_z(t)]H(y-\eta),\\
\tau_{zx}(0^+,y,t) &= \tau_{zx}(0^-,y,t),\\
D_x(0^+,y,t) &= D_x(0^-,y,t),\\
B_x(0^+,y,t) &= B_x(0^-,y,t),\\
\tau_{zy}(x,h,t) &= \tau_{zy}(x,0,t) = 0,\\
D_y(x,h,t) &= D_y(x,0,t) = 0,\\
B_y(x,h,t) &= B_y(x,h,t) = 0.
\end{aligned} \tag{15}$$

By virtue of anti-symmetry of the problem with respect to the y-axis, for the semi-infinite layer $x > 0$, condition (15) reduces to:

$$\begin{aligned}
w(0^+,y,t) &= (b_z(t)/2)H(y-\eta),\\
\bar{\phi}(0^+,y,t) &= [(b_\phi(t) - \alpha_2 b_z(t))/2]H(y-\eta),\\
\bar{\psi}(0^+,y,t) &= [(b_\psi(t) - \alpha_3 b_z(t))/2]H(y-\eta),\\
w(x,\eta^-,t) &= w(x,\eta^+,t),\\
\bar{\phi}(x,\eta^-,t) &= \bar{\phi}(x,\eta^+,t),\\
\bar{\psi}(x,\eta^-,t) &= \bar{\psi}(x,\eta^+,t),\\
\tau_{zy}(x,\eta^-,t) &= \tau_{zy}(x,\eta^+,t),
\end{aligned}$$

$$
\begin{aligned}
D_y(x,\eta^-,t) &= D_y(x,\eta^+,t),\\
B_y(x,\eta^-,t) &= B_y(x,\eta^+,t),\\
\tau_{zy}(x,h,t) &= \tau_{zy}(x,0,t) = 0,\\
D_y(x,h,t) &= D_y(x,0,t) = 0,\\
B_y(x,h,t) &= B_y(x,h,t) = 0.
\end{aligned} \tag{16}
$$

An analysis similar to that of the horizontal dislocation cut yields the solutions of the dislocation with vertical cuts. The stress, electric, and magnetic displacements in the Laplace domain are given by:

$$
\begin{aligned}
\bar{\tau}_{zx}(x,y,s) = {} & \frac{b_z(s)\tilde{c}_{44}}{\pi}\left\{\int_0^\infty\left[\frac{\omega^2\sinh(\beta(h-\eta))\cosh(\beta y)}{\beta^2\sinh(\beta h)} - \frac{e^{\omega(y-\eta)}}{2}\right]\cos(\omega x)d\omega\right.\\
& \left. - \frac{(y-\eta)}{2[x^2+(y-\eta)^2]}\right\}\\
& + \frac{b_\phi(s)e_{15} + b_\psi(s)h_{15} - (e_{15}\alpha_2 + h_{15}\alpha_3)b_z(s)}{\pi}\\
& \times\left\{\int_0^\infty\left[\frac{\sinh(\omega(h-\eta))\cosh(\omega y)}{\sinh(\omega h)} - \frac{e^{\omega(y-\eta)}}{2}\right]\right.\\
& \left.\cos(\omega x)d\omega - \frac{(y-\eta)}{2[x^2+(y-\eta)^2]}\right\}, \quad 0\le y\le\eta,\\
\bar{\tau}_{zx}(x,y,s) = {} & -\frac{b_z(s)\tilde{c}_{44}}{\pi}\left\{\int_0^\infty\left[\frac{\omega^2\sinh(\beta\eta)\cosh(\beta(h-y))}{\beta^2\sinh(\beta h)} - \frac{e^{-\omega(y-\eta)}}{2}\right]\right.\\
& \left.\cos(\omega x)d\omega + \frac{(y-\eta)}{2[x^2+(y-\eta)^2]}\right\}\\
& - \frac{b_\phi(s)e_{15} + b_\psi(s)h_{15} - (e_{15}\alpha_2 + h_{15}\alpha_3)b_z(s)}{\pi}\\
& \times\left\{\int_0^\infty\left[\frac{\sinh(\omega\eta)\cosh(\omega(h-y))}{\sinh(\omega h)} - \frac{e^{-\omega(y-\eta)}}{2}\right]\right.\\
& \left.\cos(\omega x)d\omega + \frac{(y-\eta)}{2[x^2+(y-\eta)^2]}\right\}\\
& + b_z(s)sS_T\sinh(sS_Tx), \quad \eta\le y\le h,
\end{aligned}
$$

$$
\begin{aligned}
\bar{D}_x(x,y,s) = {} & \frac{b_z(s)(d_{11}\alpha_2 + \beta_{11}\alpha_3) - b_\phi(s)d_{11} - b_\psi(s)\beta_{11}}{\pi}\\
& \times\left\{\int_0^\infty\left[\frac{\sinh(\omega(h-\eta))\cosh(\omega y)}{\sinh(\omega h)} - \frac{e^{\omega(y-\eta)}}{2}\right]\right.\\
& \left.\cos(\omega x)d\omega - \frac{(y-\eta)}{2[x^2+(y-\eta)^2]}\right\} \quad 0\le y\le\eta\\
\bar{D}_x(x,y,s) = {} & -\frac{b_z(s)(d_{11}\alpha_2 + \beta_{11}\alpha_3) - b_\phi(s)d_{11} - b_\psi(s)\beta_{11}}{\pi}\\
& \times\left\{\int_0^\infty\left[\frac{\sinh(\omega\eta)\cosh(\omega(h-y))}{\sinh(\omega h)} - \frac{e^{-\omega(y-\eta)}}{2}\right]\right.\\
& \left.\cos(\omega x)d\omega + \frac{(y-\eta)}{2[x^2+(y-\eta)^2]}\right\}, \quad \eta\le y\le h,\\
\bar{B}_x(x,y,s) = {} & \frac{b_z(s)(\beta_{11}\alpha_2 + \gamma_{11}\alpha_3) - b_\phi(s)\beta_{11} - b_\psi(s)\gamma_{11}}{\pi}
\end{aligned}
$$

$$\times \left\{ \int_0^\infty \left[\frac{\sinh(\omega(h-\eta))\cosh(\omega y)}{\sinh(\omega h)} - \frac{e^{\omega(y-\eta)}}{2} \right] \cos(\omega x) d\omega - \frac{(y-\eta)}{2[x^2+(y-\eta)^2]} \right\}, \quad 0 \le y \le \eta,$$

$$\bar{B}_x(x,y,s) = -\frac{b_z(s)(\beta_{11}\alpha_2+\gamma_{11}\alpha_3) - b_\phi(s)\beta_{11} - b_\psi(s)\gamma_{11}}{\pi} \times \left\{ \int_0^\infty \left[\frac{\sinh(\omega\eta)\cosh(\omega(h-y))}{\sinh(\omega h)} - \frac{e^{-\omega(y-\eta)}}{2} \right] \cos(\omega x) d\omega + \frac{(y-\eta)}{2[x^2+(y-\eta)^2]} \right\}, \quad \eta \le y \le h. \tag{17}$$

It can be seen from Eqs. (14) and (17) the stress field, electric, and magnetic displacement components exhibit the familiar Cauchy-type singularity at the locations of the magneto-electro-mechanical dislocation. In the case of a permeable crack, the electric and magnetic potential is continuous at the crack locations. Therefore, it is sufficient to let the jump in the electric and magnetic potential be zero in boundary conditions (9) and (16).

3 Derivation of the integral equations

In this Section, the fundamental concept of the DDT and the calculation of the numerical inversion Laplace transform are introduced. The problem is solved for a magneto-electro-elastic strip weakened by N cracks. The DDT is used by several investigators for the analyses of a cracked medium under mechanical loadings [23]. In the framework of linear theory, the present problem can be treated as the superposition of two subproblems. Sub problem I considers the strip without any cracks under action of $\tau_0 H(t)$, $D_0 H(t)$, and $B_0 H(t)$ at $y = 0, h$, and $x = \pm\infty$ for horizontal and vertical cracks, respectively, while sub problem II concerns the strip with distributed magneto-electro-mechanical dislocations on the crack faces. The sum of the two solutions corresponding to subproblems I and II is the solution to the original problem. The cracks configuration is expressed in a parametric form as follows:

$$\begin{aligned} x_i(q) &= x_i + l_i q, \\ y_i(q) &= y_i \quad i = 1, 2, \ldots, N \qquad -1 \le q \le 1 \end{aligned} \tag{18}$$

where (x_i, y_i) are the coordinates of the center of the cracks and l_i is the half-length of the cracks. Suppose that dislocations with unknown density $B_{kzj}(p,s), k \in \{m, p, \psi\}$ in the Laplace domain are distributed on the infinitesimal segment $l_j dp = \sqrt{[x_j'(p)]^2 + [y_j'(p)]^2}dp$ at the face of the j-th crack, where the parameter $-1 \le p \le 1$. Next, the superposition principle is employed to obtain the components of the stress, the electric, and the magnetic displacement on a given crack surface. The system of singular integral equations on the face of the i-th crack due to the presence of a distribution of dislocations on the face of all N horizontal cracks can be written in the following form, which will be utilized in the numerical procedure:

$$\bar{\sigma}_{yz_i}(x_i(q), y_i(q), s) = \sum_{j=1}^{N} \int_{-1}^{1} \left[\bar{K}_{ij}^{11} B_{mzj}(p,s) + \bar{K}_{ij}^{12} B_{pzj}(p,s) + \bar{K}_{ij}^{13} B_{\psi zj}(p,s) \right] l_j dp,$$

$$\bar{D}_{y_i}(x_i(q), y_i(q), s) = \sum_{j=1}^{N} \int_{-1}^{1} \left[\bar{K}_{ij}^{21} B_{mzj}(p,s) + \bar{K}_{ij}^{22} B_{pzj}(p,s) + \bar{K}_{ij}^{23} B_{\psi zj}(p,s) \right] l_j dp,$$

$$\bar{B}_{y_i}(x_i(q), y_i(q), s) = \sum_{j=1}^{N} \int_{-1}^{1} \left[\bar{K}_{ij}^{31} B_{mzj}(p,s) + \bar{K}_{ij}^{32} B_{pzj}(p,s) + \bar{K}_{ij}^{33} B_{\psi zj}(p,s) \right] l_j dp$$
$$-1 \le q \le 1, i \in \{1, 2, \ldots, N\}. \tag{19}$$

Due to Bueckner's superposition principle [24], the left-hand side of Eq. (19) represents the stress and the electro-magnetic displacement components at the presumed crack location with a negative sign, which implies the impermeable crack boundary conditions. From Eq. (14), the kernel of the integral equation (19) is given as:

$$
\begin{aligned}
\bar{K}_{ij}^{11}(q,p,s) &= \frac{\tilde{c}_{44}}{\pi}\chi_1 - \frac{(e_{15}\alpha_2 + h_{15}\alpha_3)}{\pi}\chi_2 \quad 0 \le y_i \le y_j,\\
\bar{K}_{ij}^{11}(q,p,s) &= \frac{\tilde{c}_{44}}{\pi}\chi_3 - \frac{(e_{15}\alpha_2 + h_{15}\alpha_3)}{\pi}\chi_4 \quad y_j \le y_i \le h,\\
\bar{K}_{ij}^{12}(q,p,s) &= \bar{K}_{ij}^{21}(q,p,s) = \frac{e_{15}}{\pi}\chi_2 \quad 0 \le y_i \le y_j,\\
\bar{K}_{ij}^{12}(q,p,s) &= \bar{K}_{ij}^{21}(q,p,s) = \frac{e_{15}}{\pi}\chi_4 y_j \quad \le y_i \le h,\\
\bar{K}_{ij}^{13}(q,p,s) &= \bar{K}_{ij}^{31}(q,p,s) = \frac{h_{15}}{\pi}\chi_2 0 \le y_i \le y_j,\\
\bar{K}_{ij}^{13}(q,p,s) &= \bar{K}_{ij}^{31}(q,p,s) = \frac{h_{15}}{\pi}\chi_4 y_j \le y_i \le h,\\
\bar{K}_{ij}^{22}(q,p,s) &= \frac{-d_{11}}{\pi}\chi_2 \quad 0 \le y_i \le y_j,\\
\bar{K}_{ij}^{22}(q,p,s) &= \frac{-d_{11}}{\pi}\chi_4 \quad y_j \le y_i \le h,\\
\bar{K}_{ij}^{23}(q,p,s) &= \bar{K}_{ij}^{32}(q,p,s) = \frac{-\beta_{11}}{\pi}\chi_2 \quad 0 \le y_i \le y_j,\\
\bar{K}_{ij}^{23}(q,p,s) &= \bar{K}_{ij}^{32}(q,p,s) = \frac{-\beta_{11}}{\pi}\chi_4 \quad y_j \le y_i \le h,\\
\bar{K}_{ij}^{33}(q,p,s) &= \frac{-\gamma_{11}}{\pi}\chi_2 \quad 0 \le y_i \le y_j,\\
\bar{K}_{ij}^{33}(q,p,s) &= \frac{-\gamma_{11}}{\pi}\chi_4 \quad y_j \le y_i \le h
\end{aligned}
\tag{20}
$$

where

$$
\begin{aligned}
\chi_1 = \Bigg\{ &\int_0^\infty \left[\frac{\beta \sinh(\beta(y_j - h)) \sinh(\beta y_i)}{\omega \sinh(\beta h)} + \frac{e^{-\omega(y_j - y_i)}}{2} \right] \\
&\sin(\omega(x_i - x_j + l_i q - l_j p)) d\omega \\
&- \frac{(x_i - x_j + l_i q - l_j p)}{2[(x_i - x_j + l_i q - l_j p)^2 + (y_i - y_j)^2]} \Bigg\},\\
\chi_2 = \Bigg\{ &\int_0^\infty \left[\frac{\sinh(\omega(y_j - h)) \sinh(\omega y_i)}{\sinh(\omega h)} + \frac{e^{-\omega(y_j - y_i)}}{2} \right] \\
&\sin(\omega(x_i - x_j + l_i q - l_j p)) d\omega \\
&- \frac{(x_i - x_j + l_i q - l_j p)}{2[(x_i - x_j + l_i q - l_j p)^2 + (y_i - y_j)^2]} \Bigg\},\\
\chi_3 = \Bigg\{ &\int_0^\infty \left[\frac{\beta \sinh(\beta y_j) \sinh(\beta(y_i - h))}{\omega \sinh(\beta h)} + \frac{e^{-\omega(y_i - y_j)}}{2} \right] \\
&\sin(\omega(x_i - x_j + l_i q - l_j p)) d\omega \\
&- \frac{(x_i - x_j + l_i q - l_j p)}{2[(x_i - x_j + l_i q - l_j p)^2 + (y_i - y_j)^2]} \Bigg\},\\
\chi_2 = \Bigg\{ &\int_0^\infty \left[\frac{\sinh(\omega y_j) \sinh(\omega(y_i - h))}{\sinh(\omega h)} + \frac{e^{-\omega(y_i - y_j)}}{2} \right] \\
&\sin(\omega(x_i - x_j + l_i q - l_j p)) d\omega \\
&- \frac{(x_i - x_j + l_i q - l_j p)}{2[(x_i - x_j + l_i q - l_j p)^2 + (y_i - y_j)^2]} \Bigg\}.
\end{aligned}
\tag{21}
$$

From Eq. (20), we conclude that $\bar{K}_{ij}(q, p, s)$ has the Cauchy-type singularity for $i = j$ as $p \to q$. According to the definition of the dislocation density function, the equations of the crack opening displacement, electric, and magnetic potential across the j-th crack are given by:

$$\begin{aligned}
\bar{w}_j^-(q,s) - \bar{w}_j^+(q,s) &= \int_{-1}^{q} l_j B_{mzj}(p,s)dp,\\
\bar{\phi}_j^-(q,s) - \bar{\phi}_j^+(q,s) &= \int_{-1}^{q} l_j B_{pzj}(p,s)dp,\\
\bar{\psi}_j^-(q,s) - \bar{\psi}_j^+(q,s) &= \int_{-1}^{q} l_j B_{\psi zj}(p,s)dp.
\end{aligned} \tag{22}$$

The single-valued property of the displacement field out of an embedded crack surface leads to the following closure conditions:

$$l_j \int_{-1}^{1} B_{kzj}(p,s)dp = 0 \; k \in \{m, p, \psi\}. \tag{23}$$

The numerical inversion of Laplace transform is carried out via Stehfest's method [25]. The method was used by various investigators dealing with dynamic crack problems. A time-dependent function $f(t)$ is approximated as follows:

$$f(t) \approx \frac{ln2}{t} \sum_{n=1}^{M} \upsilon_n F\left(\frac{ln2}{t} n\right). \tag{24}$$

The errors in Stehfest's method are estimated by Kuznetsov [26]. In Eq. (24), $F(.)$ is the Laplace transform of $f(t)$, M is an even number, and the coefficients υ_n are given by:

$$\upsilon_n = (-1)^{\frac{M}{2}+n} \sum_{k=[0.5(n+1)]}^{\min(\frac{M}{2},n)} \frac{k^{\frac{M}{2}}(2k)!}{(\frac{M}{2}-k)!k!(k-1)!(n-k)!(2k-n)!} \tag{25}$$

where [.] signifies the integral part of the quantity. Therefore, $f(t)$ at a fixed time t is calculated by the computation of $F(s)$ at M points $s = \frac{ln2}{t} n$, $n \in \{1, 2, \ldots, M\}$. Applying the procedure to Eqs (19) and (23) results in:

$$\begin{aligned}
\bar{\sigma}_{yz_i}\left(x_i(q), y_i(q), \frac{ln2}{t}n\right) &= \sum_{j=1}^{N} \int_{-1}^{1} \left[\bar{K}_{ij}^{11} B_{mzj}\left(p, \frac{ln2}{t}n\right) + \bar{K}_{ij}^{12} B_{pzj}\left(p, \frac{ln2}{t}n\right) + \bar{K}_{ij}^{13} B_{\psi zj}\left(p, \frac{ln2}{t}n\right)\right] l_j dp,\\
\bar{D}_{y_i}\left(x_i(q), y_i(q), \frac{ln2}{t}n\right) &= \sum_{j=1}^{N} \int_{-1}^{1} \left[\bar{K}_{ij}^{21} B_{mzj}\left(p, \frac{ln2}{t}n\right) + \bar{K}_{ij}^{22} B_{pzj}\left(p, \frac{ln2}{t}n\right) + \bar{K}_{ij}^{23} B_{\psi zj}\left(p, \frac{ln2}{t}n\right)\right] l_j dp,\\
\bar{B}_{y_i}\left(x_i(q), y_i(q), \frac{ln2}{t}n\right) &= \sum_{j=1}^{N} \int_{-1}^{1} \left[\bar{K}_{ij}^{31} B_{mzj}\left(p, \frac{ln2}{t}n\right) + \bar{K}_{ij}^{32} B_{pzj}\left(p, \frac{ln2}{t}n\right) + \bar{K}_{ij}^{33} B_{\psi zj}\left(p, \frac{ln2}{t}n\right)\right] l_j dp,\\
l_j \int_{-1}^{1} B_{kzj}\left(p, \frac{ln2}{t}n\right) dp &= 0 \quad k \in \{m, p, \psi\}, \quad i \in \{1, 2, \ldots, N\}, \quad n \in \{1, 2, \ldots, M\}.
\end{aligned} \tag{26}$$

The stress, electric, and magnetic fields at a tip of an embedded crack behave as $1/\sqrt{r}$, where r is the distance from the crack tip. Consequently, the dislocation densities are taken as:

$$B_{kzj}\left(p, \frac{ln2}{t}n\right) = \frac{G_{kzj}(p, \frac{ln2}{t}n)}{\sqrt{1-p^2}}, -1 \le p \le 1, k \in \{m, p, \psi\}, j \in \{1, 2, \ldots, N\}. \tag{27}$$

By substituting Eq. (27) into Eq. (26) and applying the numerical technique introduced by Erdogan et al. [27], the singular integral equations and the resultant equations are solved. The inverse Laplace transform of the solution from Eq. (24) leads to:

$$g_{kzj}(q,t) = \frac{ln2}{t} \sum_{n=1}^{M} \upsilon_n G_{kzi}(q, \frac{ln2}{t}n), k \in \{m, p, \psi\}, -1 \le q \le 1, i \in \{1, 2, \ldots, N\}. \tag{28}$$

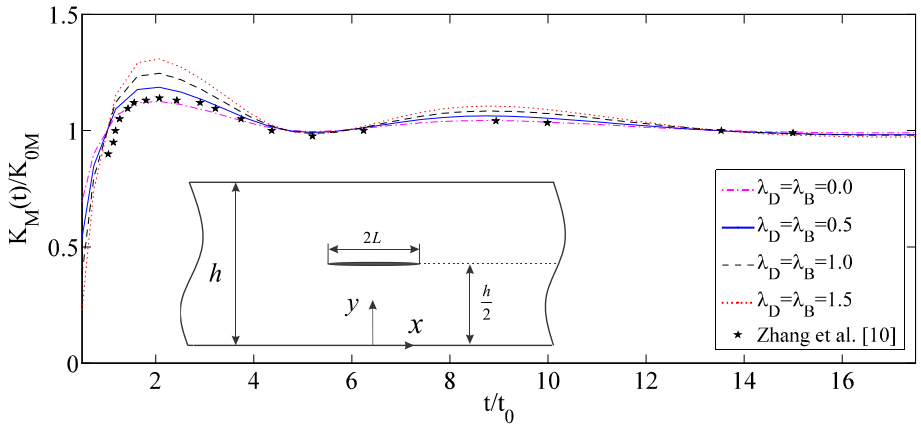

Fig. 3 The variation of the normalized DSIFs for different values of λ_D and λ_B under the impermeable assumption

The DSIFs for the embedded cracks in magneto-electro-elastic materials take the forms as follows:

$$\begin{Bmatrix}(K_M)_{Li}\\(K_M)_{Ri}\end{Bmatrix} = \pm\frac{\sqrt{l_i(\mp 1)}}{2}[c_{44}g_{mzi}(\mp 1,t)+e_{15}g_{pzi}(\mp 1,t)+h_{15}g_{\psi zi}(\mp 1,t)],$$
$$\begin{Bmatrix}(K_D)_{Li}\\(K_D)_{Ri}\end{Bmatrix} = \pm\frac{\sqrt{l_i(\mp 1)}}{2}[e_{15}g_{mzi}(\mp 1,t)-d_{11}g_{pzi}(\mp 1,t)-\beta_{11}g_{\psi zi}(\mp 1,t)],$$
$$\begin{Bmatrix}(K_B)_{Li}\\(K_B)_{Ri}\end{Bmatrix} = \pm\frac{\sqrt{l_i(\mp 1)}}{2}[h_{15}g_{mzi}(\mp 1,t)-\beta_{11}g_{pzi}(\mp 1,t)-\gamma_{11}g_{\psi zi}(\mp 1,t)] \quad (29)$$

where L and R denote the left and right tips of a crack, respectively, and $l_i(t)=\sqrt{[x_i'(t)]^2+[y_i'(t)]^2}$. Equation (28) is substituted into (29), in order to determine the field intensity factors. The details of the derivation of Eq. (29) are presented by Bagheri et al. [18].

4 Numerical results and discussion

4.1 Strip weakened by a single horizontal crack

This Section is divided into two main parts. The first deals with the verification of the resulting analytical solutions and the second with examining the influence of some prominent parameters on the dynamic field intensity factors. In what follows, we consider two special conditions, the impermeable crack and the permeable crack under impact loads. In order to determine the dynamic field intensity factors near the crack tip, the numerical results are calculated for material properties that are given in [18]. In order to analyze the effect of magneto-electro-mechanical interaction on the dynamic field intensity factors, the relation between the shear impact, the electric, and magnetic impact is defined by the loading combination parameters $\lambda_D = D_0 e_{15}/\tau_0 d_{11}$ and $\lambda_B = B_0 h_{15}/\tau_0 \beta_{11}$, respectively. In the calculations, the dynamic field intensity factors were normalized as follows:

$$\begin{bmatrix}K_{0M}\\K_{0D}\\K_{0B}\end{bmatrix} = \tau_0\sqrt{L}\begin{bmatrix}1\\d_{11}/e_{15}\\\beta_{11}/h_{15}\end{bmatrix} \quad (30)$$

where L is the half-length of the crack. In all examples in this Section, the transient response of the cracked magneto-electro-elastic strip under constant anti-plane mechanical shear $\tau_0 H(t)$, in-plane electrical loading $D_0 H(t)$, and magnetic loading $B_0 H(t)$ is studied.

Figure 3 shows the influence of the loading combination parameters on the normalized DSIFs for a central impermeable crack with variation of normalized time where $h = 0.01m$ and $L = 0.1h$. It is seen that as t/t_0 increases the normalized DSIFs first increase to maximum values and then tend to 1.0 in the end, indicating

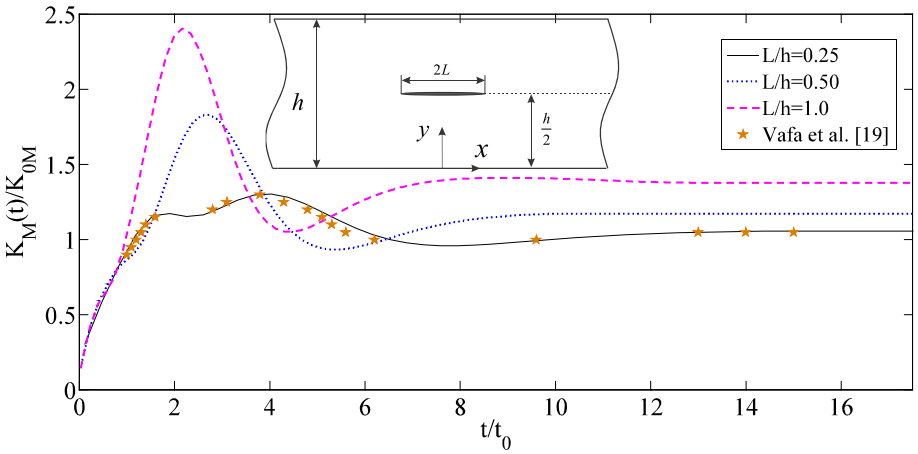

Fig. 4 Dimensionless DSIFs for different values of crack length under impermeable condition

the static value. It is shown that the peak value of the DSIFs for larger loading combination parameters is much larger than the small value. The validity of the analysis is verified by comparing our results with those available in the literature. In order to do this, a short crack in a strip without electro-magnetic properties ($\lambda_D = \lambda_B = 0$) is considered. The results for a short crack in a homogenous strip have good agreement with that reported by Zhang et al. [10] for a crack in unbounded planes.

The influences of the crack length on non-dimensional DSIFs are demonstrated graphically in Fig. 4 for the impermeable crack case. The electro-mechanical and magneto-mechanical coupling factors are zero, and the thickness of the strip is $h = 0.01m$. It turns out that, as the crack length increases, the normalized $K_M(t)/K_{0M}$ increases. This example can be easily compared with the results obtained by Vafa et al. [19]. A very good agreement is observed.

In Fig. 5, the magnitude of the normalized DSIF is plotted for three different values of the crack length for a short horizontal crack in the strip. Similar to Fig. 4, as the ratio L/y_c increases, the peak value of the DSIF will increase. In this case, the length of the crack is $L = 0.1h$. For comparison of this example, a short crack near the lower edge of a strip without magnetic properties is considered. The results in a piezoelectric strip weakened by a short crack have excellent agreement with that given by Bagheri [21] for a crack in a piezoelectric half plane, because the thickness of the strip in comparison with y_c has a high value.

In order to investigate the effects of crack surface condition and crack location on the dimensionless magnetic induction intensity factors (MIIFs), a crack under permeable and impermeable case is considered in Fig. 6. When the position of the crack is near the edge of the strip, $K_B(t)/K_{0B}$ is high. As can be observed, the normalized MIIFs are nearly independent of the normalized time for impermeable condition. This phenomenon was described by other researchers [28,29]. In contrast, for permeable condition, the MIIFs change with t/t_0. Also, it is seen that the peak value of dimensionless MIIFs for an impermeable crack is larger than the permeable one.

The effect of the strip thickness on the normalized stress and electric displacement intensity factors (EDIFs) under impermeable condition versus t/t_0 is illustrated in Fig. 7. The field intensity factors of the crack tips are increased by decreasing the thickness of the strip, and the crack would more likely extend. In fact, a maximum value for the field intensity factors of the crack tips can be observed when they are in nearest distance of the strip boundary. Also, this example implies that, for impermeable condition, the normalized EDIFs are independent of the normalized time.

4.2 Strip weakened by multiple horizontal cracks

Let us now restrict our attention to the interaction between multiple cracks. The next example is to consider the interaction between two equal-length cracks under impermeable conditions. The thickness of the strip, cracks length, and distance between two cracks centers are chosen as $h = 0.01m$, $2L = 0.5h$, and $x_{c2} - x_{c1} = 0.52h$. The variations of the normalized DSIFs versus normalized time t/t_0 are shown in Fig. 8. It can be seen that DSIFs of two interacting cracks reach a peak and then decrease in magnitude until, in the limit as t tends to infinity, the results approach the corresponding static value. As it might be observed, the DSIFs for the crack

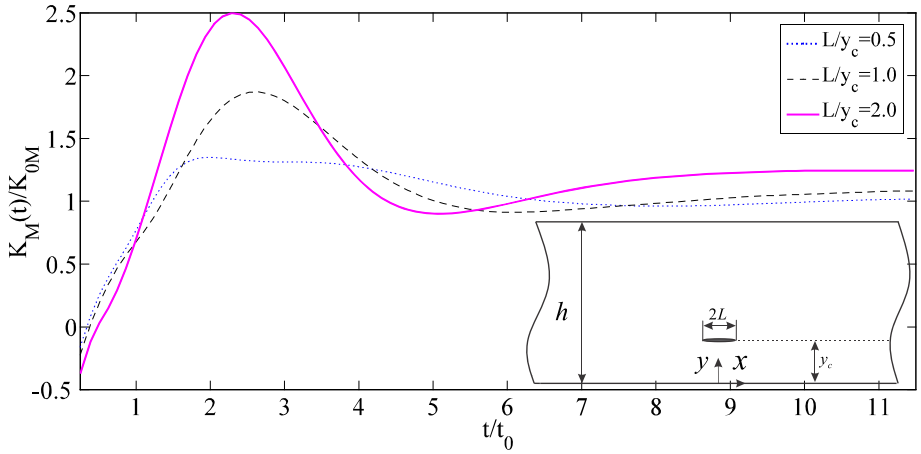

Fig. 5 Comparison of dimensionless DSIFs of a short crack in a piezoelectric strip with a crack in a piezoelectric half plane

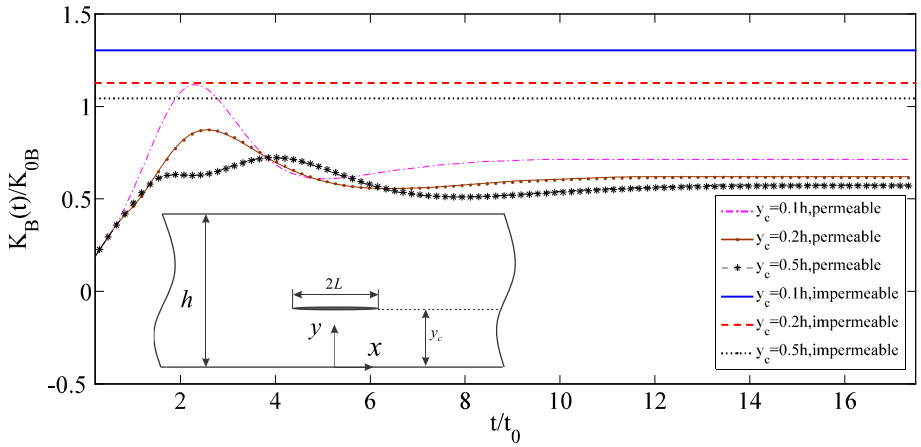

Fig. 6 Dimensionless MIIFs for permeable and impermeable conditions versus t/t_0

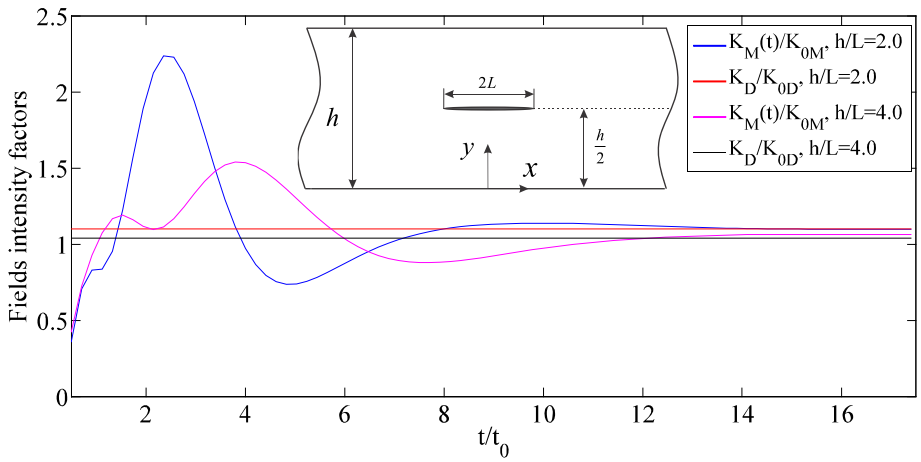

Fig. 7 Dimensionless fields intensity factors for impermeable conditions versus t/t_0

tips $R_1$and L_2 are higher than L_1 and R_2, which are attributed to the stronger interaction. A maximum value for the DSIF of the crack tips can be seen when the electro-mechanical and magneto-mechanical coupling factors increase. Also, compared with the single crack problem, higher values of the DSIF are observed due to the interaction effect between cracks.

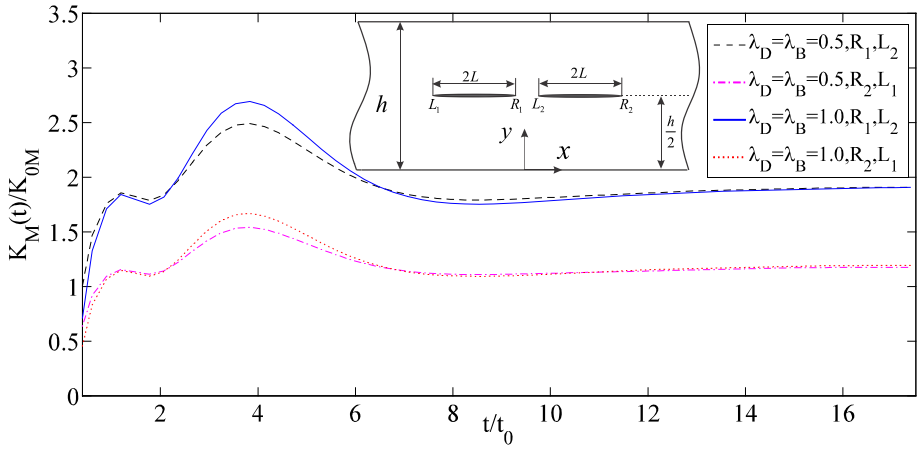

Fig. 8 The variations of the normalized DSIFs for two cracks versus t/t_0

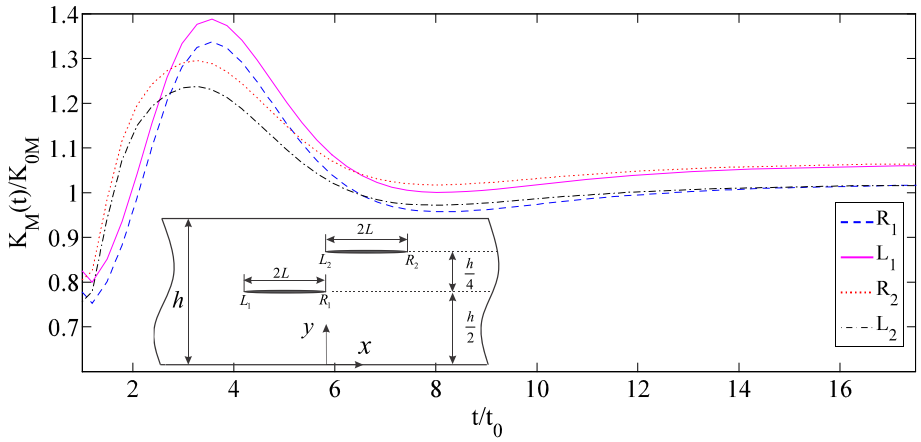

Fig. 9 The variations of the normalized DSIFs of two parallel cracks versus t/t_0

In the next example, two parallel identical cracks with the length ratio $L/h = 0.25$ are shown in Fig. 9. The effect of the cracks arrangement on the DSIFs of crack tips is determined. The distance of the crack from the strip boundary may affect the crack tip shielding or anti-shielding. On the other hand, for L_1R_1, the DSIFs for the crack tips are more than L_2R_2.

4.3 Strip weakened by a vertical embedded crack

In Fig. 10, the magnitude of the normalized DSIF is plotted with respect to t/t_0 for a vertical crack. In this case, we let all the magnetic quantities be zero for the case of a piezoelectric strip. In this example, the center of the crack is located at $y_c/h = 0.5$. Note that, as λ_D increases, the DSIFs of the crack tips increase. Our results are in good agreement with the existing results given by Yong and Zhou [14].

4.4 Strip weakened by multiple vertical embedded cracks

Figure 11 shows the variation of normalized DSIFs in a magneto-electro-elastic strip containing two straight vertical cracks L_1R_1 and L_2R_2 with equal-length $2L = 0.4h$. As the distance x_{c2} increases, the normalized DSIFs decrease. It may again be seen that the results are highly dependent on the interaction of the cracks.

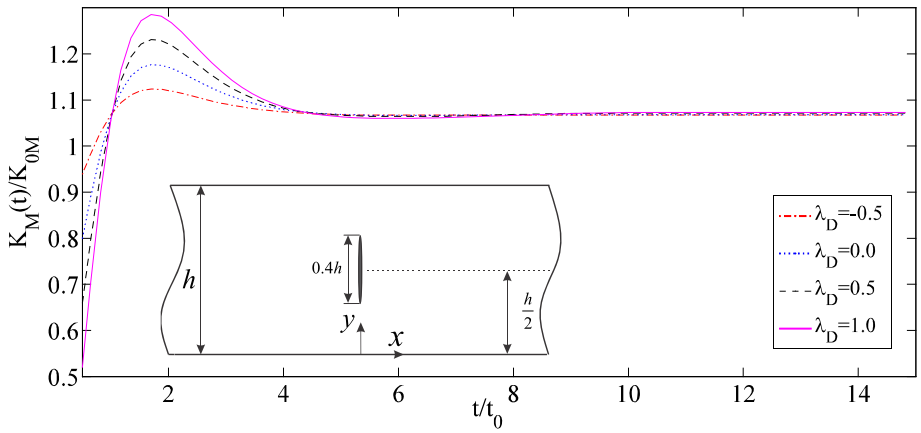

Fig. 10 The variations of the normalized DSIFs of a vertical crack versus t/t_0

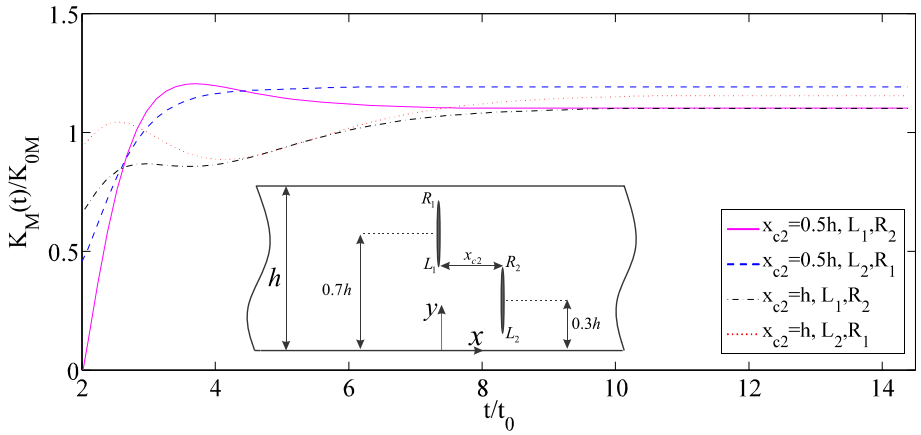

Fig. 11 The variations of the normalized DSIFs of two vertical cracks versus t/t_0

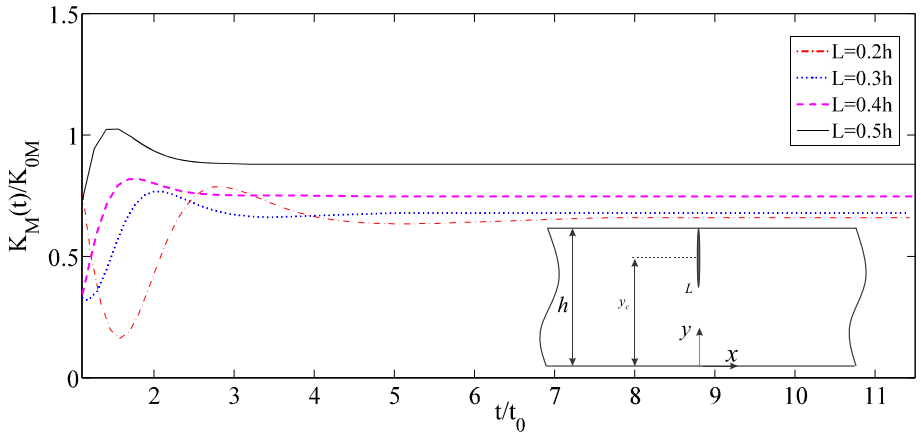

Fig. 12 The variations of the normalized DSIF of an edge crack versus t/t_0

4.5 Strip weakened by a vertical edge crack

In the next example, an edge crack in the strip with length ratio $L/h = 0.2, 0.3, 0.4, 0.5$ is considered. The result depicts the effects of the crack length on the normalized DSIF, $K_M(t)/K_{0M}$ wherein L designates the embedded tip of the crack. It can be seen that the DSIFs increase rapidly as the crack length increases (Fig. 12).

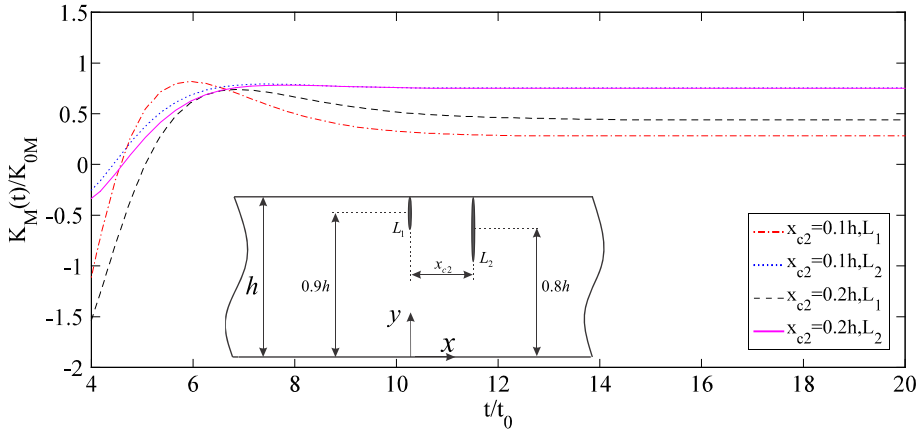

Fig. 13 The variations of the normalized DSIFs of two edge cracks versus t/t_0

4.6 Strip weakened by multiple vertical edge cracks

In the last example, for two edge cracks, the variations of the normalized DSIFs versus the normalized time are examined in Fig. 13. The results show that the DSIFs are highly dependent on the distance of the cracks. Generally, as the crack length increases or the distance crack tip from the strip edge decreases, the normalized DSIFs increase. In this example, the effect of the distance crack tip from the strip edge on $K_M(t)/K_{0M}$ can be very significant for the crack length. In other words, for L_1, the DSIFs for the crack tips are more than L_2.

5 Conclusions

The purpose of this study is to investigate the effects of the crack configurations and arrangements on the field intensity factors in a magneto-electro-elastic strip under anti-plane shear impact loading. The impermeable or permeable conditions along the crack surface are assumed. We develop the DDT which can be used for an analysis of the multiple horizontal, vertical, and edge cracks in a strip. The solutions of dislocations are derived in the magneto-electro-elastic strip using the Fourier and Laplace transform methods. These solutions are utilized to construct integral equations for the cracked strip. Finally, the effects of the crack length, geometrical parameter, and the cracks configuration on the field intensity factors are studied. In summary, some conclusions are drawn as follows:

(i) The geometric size of the strip has significant influence on the field intensity factors for both impermeable and permeable cases.
(ii) Results show that the field intensity factors are influenced by the applied magneto-electric and mechanical loadings and the type of magneto-electric boundary conditions along the crack faces.
(iii) The curves of field intensity factors increase with time, reach a peak value, and then drop to a steady state which is in accordance with the known results for the transient analysis of a cracked magneto-electro-elastic material.
(iv) For impermeable condition, the normalized EDIFs and MIIFs are independent of the normalized time but for permeable case the EDIFs and MIIFs change with t/t_0.

Appendix

The unknown coefficients in (11) may be determined as:

$$A_1(\omega, s) = A_2(\omega, s) = -\frac{b_z(s)[\pi\delta(\omega) - i/\omega]\sinh(\beta(h-\eta))e^{-i\omega\zeta}}{2\sinh(\beta h)},$$

$$A_3(\omega, s) = \frac{b_z(s)[\pi\delta(\omega) - i/\omega]\sinh(\beta\eta)e^{\beta h}e^{-i\omega\zeta}}{2\sinh(\beta h)},$$

$$A_4(\omega,s)=\frac{b_z(s)[\pi\delta(\omega)-i/\omega]\sinh(\beta\eta)e^{-\beta h}e^{-i\omega\zeta}}{2\sinh(\beta h)},$$

$$B_1(\omega,s)=B_2(\omega,s)=-\frac{[b_\phi(s)-\alpha_2 b_z(s)][\pi\delta(\omega)-i/\omega]\sinh(|\omega|\,(h-\eta))e^{-i\omega\zeta}}{2\sinh(|\omega|\,h)},$$

$$B_3(\omega,s)=\frac{[b_\phi(s)-\alpha_2 b_z(s)][\pi\delta(\omega)-i/\omega]\sinh(|\omega|\,\eta)e^{|\omega|h}e^{-i\omega\zeta}}{2\sinh(|\omega|\,h)},$$

$$B_4(\omega,s)=\frac{[b_\phi(s)-\alpha_2 b_z(s)][\pi\delta(\omega)-i/\omega]\sinh(|\omega|\,\eta)e^{-|\omega|h}e^{-i\omega\zeta}}{2\sinh(|\omega|\,h)},$$

$$C_1(\omega,s)=C_2(\omega,s)=-\frac{[b_\psi(s)-\alpha_3 b_z(s)][\pi\delta(\omega)-i/\omega]\sinh(|\omega|\,(h-\eta))e^{-i\omega\zeta}}{2\sinh(|\omega|\,h)},$$

$$C_3(\omega,s)=\frac{[b_\psi(s)-\alpha_3 b_z(s)][\pi\delta(\omega)-i/\omega]\sinh(|\omega|\,\eta)e^{|\omega|h}e^{-i\omega\zeta}}{2\sinh(|\omega|\,h)},$$

$$C_4(\omega,s)=\frac{[b_\psi(s)-\alpha_3 b_z(s)][\pi\delta(\omega)-i/\omega]\sinh(|\omega|\,\eta)e^{-|\omega|h}e^{-i\omega\zeta}}{2\sinh(|\omega|\,h)}.$$

References

1. Zhou, Z.G., Wu, L.Z., Wang, B.: The behavior of a crack in functionally graded piezoelectric/piezomagnetic materials under anti-plane shear loading. Arch. Appl. Mech. **74**, 526–535 (2005)
2. Fotuhi, A.R., Fariborz, S.J.: Anti-plane analysis of a functionally graded strip with multiple cracks. Int. J. Solids Struct. **43**, 1239–1252 (2006)
3. Tupholme, G.E.: Magnetoelectroelastic media containing a row of moving shear cracks. Mech. Res. Commun. **45**, 48–53 (2012)
4. Rokne, J., Singh, B.M., Dhaliwal, R.S.: Moving anti-plane shear crack in a piezoelectric layer bonded to dissimilar elastic infinite spaces. Eur. J. Mech. A Solids **31**, 47–53 (2012)
5. Fu, J., Hu, K., Chen, Z., Chen, L., Qian, L.: A moving crack propagating in a functionally graded magnetoelectroelastic strip under different crack face conditions. Theor. Appl. Fract. Mech. **66**, 16–25 (2013)
6. Mousavi, S.M., Paavola, J.: Analysis of functionally graded magneto-electro-elastic layer with multiple cracks. Theor. Appl. Fract. Mech. **66**, 1–8 (2013)
7. Chen, Z.T., Karihaloo, B.L.: Dynamic response of a cracked piezoelectric ceramic arbitrary electro-mechanical impact. Int. J. Solids Struct. **36**, 5125–5133 (1999)
8. Li, X.F.: Transient response of a piezoelectric material with a semi-infinite mode-III crack under impact loads. Int. J. Fract. **111**, 119–130 (2001)
9. Gu, B., Wang, X., Yu, S.W., Gross, D.: Transient response of Griffith crack between dissimilar piezoelectric layers under anti-plane mechanical and in-plane electrical impacts. Eng. Fract. Mech. **69**, 565–576 (2002)
10. Zhang, Ch., Sladek, J., Sladek, V.: Effects of material gradients on transient dynamic mode-III stress intensity factors in a FGM. Int. J. Solids Struct. **40**, 5251–5270 (2003)
11. Li, X.F.: Dynamic analysis of a cracked magnetoelectroelastic medium under antiplane mechanical and inplane electric and magnetic impacts. Int. J. Solids Struct. **42**, 3185–3205 (2005)
12. Feng, W.J., Su, R.K.L.: Dynamic internal crack problem of a functionally graded magneto-electro-elastic strip. Int. J. Solids Struct. **43**, 5196–5216 (2006)
13. Su, R.K.L., Feng, W.J., Liu, J.: Transient response of interface cracks between dissimilar magneto-electro-elastic strips under out-of-plane mechanical and in-plane magneto-electrical impact loads. Compos Struct. **78**, 119–128 (2007)
14. Yong, H.D., Zhou, Y.H.: Transient response of a cracked magnetoelectroelastic strip under anti-plane impact. Int. J. Solids Struct. **44**, 705–717 (2007)
15. García-Sánchez, F., Zhang, Ch., Sáez, A.: 2-D transient dynamic analysis of cracked piezoelectric solids by a time-domain BEM. Comput. Methods Appl. Mech. **197**, 3108–3121 (2008)
16. Chen, X.: Dynamic crack propagation in a magneto-electro-elastic solid subjected to mixed loads: transient mode-III problem. Int. J. Solids Struct. **46**, 4025–4037 (2009)
17. Monfared, M.M., Ayatollahi, M.: Dynamic stress intensity factors of multiple cracks in an orthotropic strip with FGM coating. Eng. Fract. Mech. **109**, 45–57 (2013)
18. Bagheri, R., Ayatollahi, M., Mousavi, S.M.: Stress analysis of a functionally graded magneto-electro-elastic strip with multiple moving cracks. Math. Mech. Solids **22**, 304–323 (2015)
19. Vafa, J.P., Baghestani, A.M., Fariborz, S.J.: Transient screw dislocation in exponentially graded FG layers. Arch. Appl. Mech. **85**, 1–11 (2015)
20. Hassani, A.R., Monfared, M.M.: Analysis of an orthotropic circular bar weakened by multiple radial cracks under torsional transient loading. Eng. Fract. Mech. (in press, accepted manuscript) (2017)
21. Bagheri, R.: Several horizontal cracks in a piezoelectric half-plane under transient loading. Arch. Appl. Mech. **87**, 1979–1992 (2017)

22. Bleustein, J.L.: A new surface wave in piezoelectric materials. Appl. Phys. Lett. **13**, 412–413 (1968)
23. Weertman, J.: Dislocation Based Fracture Mechanics. World Scientific, Singapore (1996)
24. Korsunsky, A.M., Hills, D.A.: The solution of crack problems by using distributed strain nuclei. Proc. Inst. Mech. Eng. Part C J. Mech. Eng. Sci. **210**, 23–31 (1996)
25. Cohen, A.M.: Numerical Methods for Laplace Transform Inversion. Springer, Berlin (2007)
26. Kuznetsov, A.: On the convergence of the Gaver–Stehfest algorithm. SIAM. J. Numer. Anal. **51**, 2984–2998 (2013)
27. Erdogan, F., Gupta, G.D., Cook, T.S.: Numerical solution of integral equations. In: Sih, G.C. (ed.) Methods of Analysis and Solution of Crack Problems, pp. 368–425. Noordhoof, Leyden (Holland) (1973)
28. Garcı'a-Sa'nchez, F., Zhang, Ch., Sla'dek, J., Sla'dek, V.: 2D transient dynamic crack analysis in piezoelectric solids by BEM. Comput. Mater. Sci. **39**, 179–186 (2007)
29. Feng, W.J., Li, Y.S., Xu, Z.H.: Transient response of an interfacial crack between dissimilar magnetoelectroelastic layers under magnetoelectromechanical impact loadings: Mode-I problem. Int. J. Solids Struct. **46**, 3346–3356 (2009)